Episodic synchronization in dynamically driven neurons

Pablo Balenzuela,[1,2,*] Javier M. Buldú,[1,3] Marcos Casanova,[1] and Jordi García-Ojalvo[1,†]
[1]*Departament de Física i Enginyeria Nuclear, Universitat Politècnica de Catalunya, Colom 11, E-08222 Terrassa, Spain*
[2]*Departamento de Física, Facultad de Ciencias Exactas y Naturales, Universidad de Buenos Aires, Pabellón 1, Ciudad Universitaria (1428), Buenos Aires, Argentina*
[3]*Nonlinear Dynamics and Chaos Group, Departamento de Ciencias de la Naturaleza y Física Aplicada, Universidad Rey Juan Carlos, Tulipán s/n, 28933 Móstoles, Madrid, Spain*
(Received 10 May 2006; revised manuscript received 13 October 2006; published 26 December 2006)

We examine the response of type II excitable neurons to trains of synaptic pulses, as a function of the pulse frequency and amplitude. Similarly to the case of harmonic inputs, these neurons exhibit a resonant behavior also for pulsed inputs. We interpret this phenomenon in terms of the subthreshold response of the neuron. In the presence of dynamical trains of input pulses whose frequency varies continuously in time, the receiving neuron synchronizes episodically to the input pulses, whenever the pulse frequency lies within the neuron's locking range. The results are obtained both in numerical simulations of the Morris-Lecar model and in an electronic implementation of the FitzHugh-Nagumo system, evidencing the robustness of the phenomenon.

DOI: 10.1103/PhysRevE.74.061910 PACS number(s): 87.19.La, 05.45.Xt, 87.10.+e

I. INTRODUCTION

Neurons exhibit all-or-none responses to external input signals. The main function of this thresholding behavior is to process information in a way that is efficient and robust to noise [1]. Input signals received by most nonsensory neurons take the form of pulse trains, coming from the spiking activity of neighboring neurons. Therefore, in order to understand the mechanisms of information processing in neural systems, it is very important to characterize in detail the response of neurons to pulse trains. Furthermore, realistic pulse trains are intrinsically dynamical, with an instantaneous firing frequency that varies continuously in time. It is therefore necessary to assess the influence of this nonstationarity in the neuronal response. This paper addresses these questions.

Most studies of driven neurons have been restricted so far to harmonic driving signals [2–6]. Many of these works have shown that for certain types of neurons, i.e., those exhibiting what is called type II excitability, a resonant behavior arises with respect to the external driving frequency [7–9]. Excitability in those neurons is usually associated with an Andronov-Hopf bifurcation, which leads to the existence of subthreshold oscillations in the excitable regime. When the frequency of these oscillations equals that of the harmonic driving, a resonance arises.

A similar resonant behavior exists for pulsed inputs. In that case, the same pulse train impinging on two different neurons can elicit a response on only one of them, i.e., on the one that is tuned to resonate with the incoming pulse frequency. Izhikevich and co-workers [10–12] proposed this type of phenomenon as a mechanism for selective multiplexed communication, whereby a single neural channel can be used to transmit multiple signals, each of which is detected by distinct groups of neurons depending on their interspike frequency. Here we pursue this idea further, analyzing the resonant behavior in terms of the subthreshold response of the neuron. We also show that this behavior leads to episodic synchronization between the neuron's output and an input with dynamically varying firing rate. Episodic synchronization has previously been reported in coupled lasers with intrinsic dynamics [13]. Here we extend that property to externally driven excitable systems. Two types of systems have been investigated: a Morris-Lecar model (Sec. II) and an electronic implementation of the FitzHugh-Nagumo model (Sec. III). The Morris-Lecar model is chosen as a compromise between a realistic representation of neuronal dynamics and an analytically tractable system. Furthermore, this model has the advantage that types I and II excitability can be obtained with a single parameter change (see Table 1 below). We use the FitzHugh-Nagumo circuit, on the other hand, with two goals: (i) to show that the reported results are independent of the particular model used, and (ii) to test the intrinsic robustness of the behavior in an experimental setting where noise and parameter mismatches between the input and output circuits are unavoidable.

II. MORRIS-LECAR MODEL

A. Model description

We consider neurons whose dynamical behavior is described by the Morris-Lecar model [14],

$$\frac{dV}{dt} = \frac{1}{C_m}(I_{\text{app}} - I_{\text{ion}} - I_{\text{syn}}) + D\xi(t), \tag{1}$$

$$\frac{dW}{dt} = \phi\Lambda(V)[W_\infty(V) - W], \tag{2}$$

where V and W represent the membrane potential and the fraction of open potassium channels, respectively. C_m is the membrane capacitance per unit area and ϕ is the decay rate of W. The neuron is affected by several currents, including an external current I_{app}, a synaptic current I_{syn}, and an ionic current given by

*Electronic address: balen@df.uba.ar
†Electronic address: jordi.g.ojalvo@upc.edu

TABLE I. Parameter values of the Morris-Lecar and synapse models used in this work.

Parameter	Morris-Lecar TII (TI)
C_m	5 μF/cm^2
g_K	8 mS/cm^2
g_L	2 mS/cm^2
g_{Ca}	4.0 mS/cm^2
V_K^0	−80 mV
V_L^0	−60 mV
V_{Ca}^0	120 mV
V_{M1}	−1.2 mV
V_{M2}	18 mV
V_{W1}	2 mV (12 mV)
V_{W2}	17.4 mV
ϕ	1/15 ms^{-1}
Parameter	**Synapse**
α	2.0 ms^{-1} mM^{-1}
β	1.0 ms^{-1}
$T_{\max}$	1.0 mM
g_{syn}	(specified in each case)
τ_{syn}	1.5 ms
E_s	0 mV

$$I_{\text{ion}} = g_{\text{Ca}} M_\infty(V)(V - V_{\text{Ca}}^0) + g_{\text{K}} W(V - V_{\text{K}}^0) + g_L(V - V_L^0). \tag{3}$$

In this expression, g_a (a=Ca,K,L) are the conductances and V_a^0 the resting potentials of the calcium, potassium and leaking channels, respectively. We define the following functions of the membrane potential:

$$M_\infty(V) = \frac{1}{2}\left[1 + \tanh\left(\frac{V - V_{M1}}{V_{M2}}\right)\right], \tag{4}$$

$$W_\infty(V) = \frac{1}{2}\left[1 + \tanh\left(\frac{V - V_{W1}}{V_{W2}}\right)\right], \tag{5}$$

$$\Lambda(V) = \cosh\left(\frac{V - V_{W1}}{2V_{W2}}\right), \tag{6}$$

where V_{M1}, V_{M2}, V_{W1}, and V_{W2} are constants to be specified later. The last term in Eq. (1) is a white Gaussian noise term of zero mean and amplitude D and takes into account the synaptic background in which a neuron is embedded.

In the absence of noise, an isolated Morris-Lecar neuron shows a bifurcation to a limit cycle for increasing applied current I_{app} [6]. Depending on the parameters, this bifurcation can be of the saddle-node or the subcritical Hopf types, corresponding to either type I or type II excitability, respectively. The specific values of the parameters used are shown in Table I [15]. For these parameters, the threshold values of the applied current under constant stimulation are 39.7 μA/cm^2 for type I and 46.8 μA/cm^2 for type II.

In this paper we analyze the behavior of a neuron driven by a synaptic current. To that end, we use the simplified model of chemical synapse proposed in [16], according to which the synaptic current is given by

$$I_{\text{syn}} = g_{\text{syn}} r(t)(V - E_s), \tag{7}$$

where g_{syn} is the conductance of the synaptic channel, $r(t)$ represents the fraction of bound receptors, and E_s is a parameter whose value determines the type of synapse: if E_s is larger than the rest potential the synapse is excitatory, if smaller it is inhibitory; here we consider an excitatory synapse with E_s=0 mV. The fraction of bound receptors, $r(t)$, follows the equation

$$\frac{dr}{dt} = \alpha[T](1 - r) - \beta r, \tag{8}$$

where $[T] = T_{\max}\theta(T_0 + \tau_{\text{syn}} - t)\theta(t - T_0)$ is the concentration of neurotransmitter released into the synaptic cleft by the presynaptic neuron, whose dynamics is also given by Eqs. (1) and (2) with no synaptic input. α and β are rise and decay time constants, respectively, and T_0 is the time at which the presynaptic neuron fires, which happens whenever the presynaptic membrane potential exceeds a predetermined threshold value, in our case chosen to be 10 mV. This thresholding mechanism lies at the origin of the nonlinear character of the synaptic coupling. The time during which the synaptic connection is active is roughly given by τ_{syn}. The values of the coupling parameters that we use [16] are specified in Table I. The equations were integrated using the Heun method [17], which is a second order Runge-Kutta algorithm for stochastic equations.

B. Response diagram of a periodically driven neuron

First we analyze how a Morris-Lecar neuron responds to periodic inputs of varying frequencies. Specifically, we ask how large the signal needs to be in order to elicit spikes in the receiving neuron. It is also important to characterize the frequency of spiking in terms of frequency of the input. As mentioned in the Introduction, this question has already been addressed, in the case of harmonic inputs, for different neuronal models, including the Morris-Lecar model [18]. We will now compare these results with those obtained for a pulsed input. For the Morris-Lecar model, one can expect a completely different behavior between the type I and the type II cases, given that the bifurcation to a limit cycle is a saddle-node bifurcation in the former case and a Hopf bifurcation (with the well-known eigenfrequency associated to the spiral fixed point) in the latter.

We first consider an isolated neuron without synaptic inputs (I_{syn}=0), but subject to a harmonic modulation of the applied current I_{app} with the form,

$$I_{\text{app}} = I_0 + A\cos(2\pi f_{\text{in}} t). \tag{9}$$

In order to quantify the response of the neuron to this harmonic input, we plot in Fig. 1 (in grayscale) the ratio between the output and the input frequencies, $f_{\text{out}}/f_{\text{in}}$, as a function of the amplitude A and frequency f_{in} of the applied

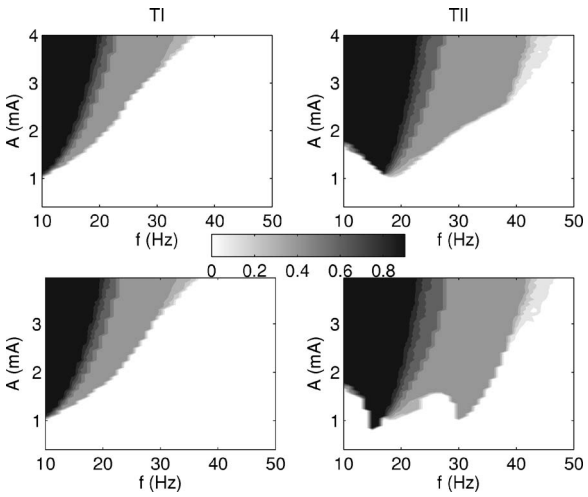

FIG. 1. Response diagram of Morris Lecar neurons for a harmonic input: f_{out}/f_{in} is plotted in greyscale as a function of the amplitude and frequency of the applied current. Left plots: type I neuron (with $I_0=39\ \mu A/cm^2$); right plots: type II neuron (with $I_0=46\ \mu A/cm^2$). The response is measured for increasing A in the upper plots, and for decreasing A in the lower plots.

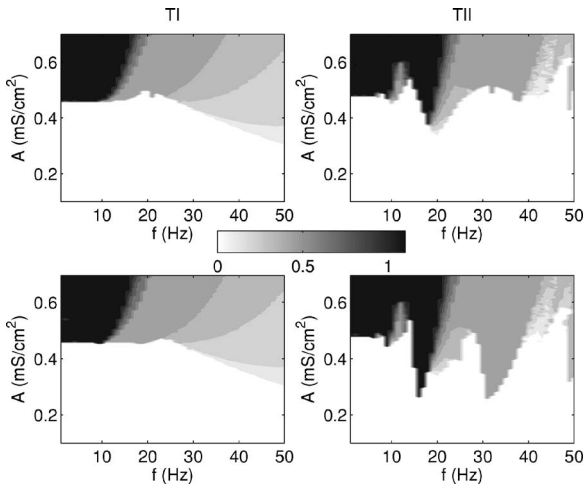

FIG. 2. Response diagrams of Morris Lecar neurons to a periodic synaptic (pulsed) input: f_{out}/f_{in} is plotted (in greyscale scale) as a function of the amplitude and the frequency of the synaptic current. Left plots: type I neuron (with $I_{app}=39\ \mu A/cm^2$); right plots: type II neuron (with $I_{app}=46\ \mu A/cm^2$). The response is measured for increasing A in the upper plots, and for decreasing A in the lower plots.

current (9). The figure compares the resulting *response diagrams* of type I and type II neurons. To obtain these plots, A is varied for fixed f, while using as initial condition for a given A the final state of the previous A value. In the upper panels A increases, thus showing the stability of the rest state, while in the lower panels A decreases, this indicating the stability of the limit cycle. The figure shows that type II neurons have a region of bistability, where the fixed point and the limit cycle coexist. In contrast, for type I neurons the two plots are basically the same, indicating an absence of bistability.

There is another qualitative difference between types I and II that can be observed in Fig. 1. In the type I neuron, the critical modulation amplitude for spiking increases monotonically with the frequency of the stimulus. On the other hand, in the type II neuron the critical amplitude exhibits a minimum for a given nonzero frequency, in our case around 20 Hz. This behavior can be understood as resulting from the subthreshold damped oscillations characteristic of type II excitability [6].

We now characterize the response of a neuron to an input train of periodic synaptic pulses of varying frequencies and amplitudes. To that end, we drive the neuron with the synaptic current Eq. (7), with $g_{syn}=A$ and the dynamics of $r(t)$ being described by Eq. (8) with presynaptic firings occurring periodically with frequency f_{in}. In this way, we can quantify the response of the neuron in terms of the efficiency in responding to a periodic synaptic input with a given frequency and amplitude, as shown above in the harmonic case. Figure 2 shows the corresponding response diagrams, i.e., f_{out}/f_{in} as a function of A and f_{in}, for both excitability types and for increasing (top) and decreasing (bottom) A. The behavior shows features common to the harmonic case, such as the existence of the same resonant frequency in type II for both kinds of inputs. But there are also very interesting differences between them, especially in the high and zero frequency limits.

The main difference between the harmonic and pulsed input cases is the approach to the DC threshold current ($39.7\ \mu A/cm^2$ for type I and $46.8\ \mu A/cm^2$ for type II). While in the former case this happens for frequencies approaching zero (type I) or resonance (type II), for pulsed inputs it happens for high frequencies, i.e., when the signal period is of the order of the pulse width. This is the reason for the appearance of a spiking region at high frequencies for pulsed inputs, which is absent in the harmonic case [19]. Also, in the low-frequency limit one can observe, for pulsed inputs, a constant value of the critical amplitude. This is related with the fact that, when the input period is high enough with respect to the pulse width, the system response is essentially independent of the period.

C. Subthreshold dynamics

Experimental studies have shown that when the membrane potential of a type II neuron is driven by a small oscillatory current in the subthreshold regime, it exhibits a preferred response to certain input frequencies [20–24]. The connection between subthreshold resonance and firing frequency preferences was studied, for the case of harmonic driving, in [8,9]. With this in mind, we have analyzed the subthreshold dynamics of the Morris-Lecar model, both for harmonic and pulsed applied currents [25]. Below threshold, the model Eqs. (1) and (2) (without noise and synaptic current) can be linearized around its stationary solution, and an approximate solution can be obtained for small stimulus amplitude. For a harmonic input, i.e., $I_{ext}=I_1\sin(\omega t)$ with $\omega=2\pi f$, one can calculate the impedance as a function of the input frequency as $Z(\omega)=\frac{|V(t)|}{|I(t)|}$, where $|\cdots|$ denote the root-mean-square (RMS) value of the signal. Except for a constant factor, the impedance can be expressed as

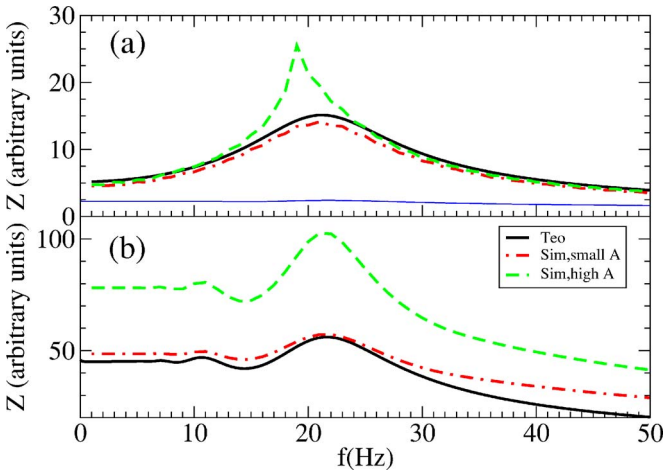

FIG. 3. (Color online) Impedance for subthreshold harmonic (a) and pulsed (b) input current from theoretical calculations (solid line) and simulations for small [$A=0.5\ \mu\mathrm{A/cm^2}$ in (a) and $A=0.01\ \mathrm{mS/cm^2}$ in (b)] and high amplitude [$A=0.9\ \mu\mathrm{A/cm^2}$ in (a) and $A=0.1\ \mathrm{mS/cm^2}$ in (b)] of the stimuli (dashed-dotted and dashed lines, respectively). In (a), the black curve corresponds to Eq. (10); in (b) it corresponds to Eq. (13).

$$Z(\omega) = \sqrt{\frac{d^2+\omega^2}{b^2c^2+2bc(\omega^2-ad)+(a^2+\omega^2)(d^2+\omega^2)}}, \tag{10}$$

where a and b represent the partial derivatives of the right-hand side of Eq. (1) with respect to V and W, respectively, while c and d are the corresponding derivatives of the right-hand side of Eq. (2).

For parameters corresponding to a type II neuron, $Z(\omega)$ displays a maximum at a given frequency f_{res} [Fig. 3(a)], indicating that, for small departures from resting state, the subthreshold membrane potential has maximal response at that frequency. For the parameters chosen in this work, $f_{\mathrm{res}} \simeq 21$ Hz, while the minimum in the response diagram for harmonic inputs (Fig. 1, right) is $f \simeq 19$ Hz. This difference is due to the small amplitude approximation, as can be seen in Fig. 3(a), which compares the theoretical result (10) with numerical simulations of model Eqs. (1) and (2) for two different ampitudes of the input current (always in the subthreshold regime). The figure shows that the larger that amplitude, the larger the deviation of the impedance maximum from the linearized calculations.

If the external current I_{ext} is not harmonic but pulsed, we can write it in terms of its Fourier series:

$$I_{\mathrm{ext}}(t) = I_1 \sum_{k=-\infty}^{\infty} \alpha_k e^{ik\omega t}. \tag{11}$$

Solving the linearized model of Eqs. (1) and (2) for each Fourier component of this input current, one can obtain an impedance $Z_k(\omega)$ from Eq. (10) for each component, and find the membrane potential for small departures from its resting state:

$$v(t) = I_1 \sum_{k=-\infty}^{\infty} \alpha_k Z_k(\omega) e^{ik\omega t}, \tag{12}$$

where $v = V - V_{st}$. Dividing the RMS values of Eqs. (12) and (11) leads to the total impedance of the system in this case which reads

$$Z(\omega) = \sqrt{\frac{\sum_{k=-\infty}^{\infty} Z_k^2(\omega)\alpha_k^2}{\sum_{k=-\infty}^{\infty} \alpha_k^2}}. \tag{13}$$

In the subthreshold dynamics, the shape of the synaptic pulses can be reasonably well approximated by square pulses. For a train of rectangular pulses of width τ and period $2\pi/\omega$, the Fourier coefficients are $\alpha_k = \frac{i}{2\pi k}(e^{-ik\omega\tau}-1)$. We calculated the theoretical prediction of the impedance for rectangular pulses of width $\tau=5$ ms, taking the Fourier series up to $k=10\,000$ in Eq. (13). The result is plotted as a black curve in Fig. 3(b). That figure also shows the results from numerical simulations for synaptic inputs given by Eq. (8) at two values of the driving amplitude. Again, the subthreshold response shows a maximum at the frequency f_{res} corresponding to the fundamental frequency, but it also shows a second local maximum at the frequency $f_{\mathrm{res}}/2$ corresponding to first subharmonic. This local maximum at $f_{\mathrm{res}}/2$ also appears in the theoretical prediction of the impedance calculated from Eq. (13). The agreement obtained between simulation results and the theoretical prediction from Eq. (13), supports the approximation of synaptic pulses by square pulses of similar width in the low-amplitude subthreshold regime.

D. The dynamical case: Variation of the input frequency

In previous sections, we have characterized the behavior of a neuron subject to a pulsed synaptic current of fixed frequency. Our results corroborate that type II neurons exhibit a resonant behavior, defined by the existence of an optimal frequency for which the critical amplitude of spiking is minimal. The question now is, what happens if the frequency of the input train varies dynamically, which is a more realistic situation for a nonsensory neuron. This kind of stimulus, in the subthreshold regime, is commonly used to measure the subthreshold behavior of a neuron and is referred to as ZAP [impedance (Z)-Amplitude-Profile] stimulus. Here we consider the case where the stimulus is not subthreshold, and examine the dependence of the neuron's response on the variation rate of the input frequency.

To address this issue, we made simulations with two Morris-Lecar neurons coupled unidirectionally through a chemical synapse. The input neuron operates in the limit cycle regime and is considered to be type I, so that we can control its spiking frequency by varying its applied current I_{app} [6]. This neuron is synaptically coupled to a type II neuron operating in an excitable regime, with a coupling strength g_{syn} such that the receiving neuron only fires in a given range of frequencies (i.e., the coupling is such that the amplitude of the input pulses lies below the critical ampli-

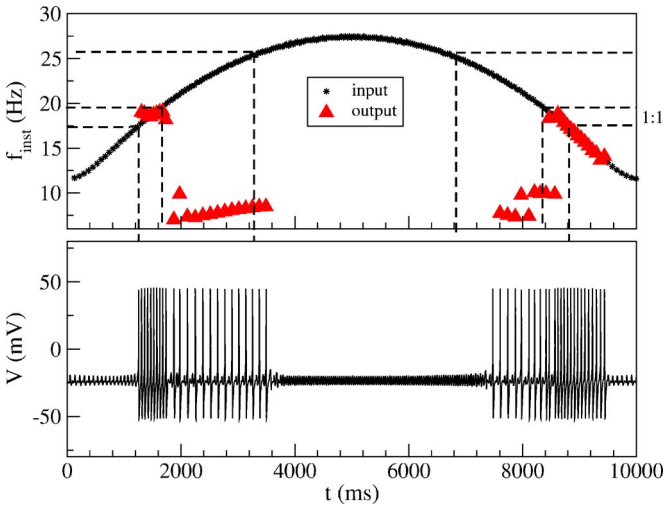

FIG. 4. (Color online) Upper plot: instantaneous frequency versus time of the input neuron (black stars) and of the receiving neuron (triangles). The three horizontal dashed lines indicate the boundaries of the locking region for the selected synaptic strength (g_{syn}=0.43 mS/cm^2); the 1:1 region is specifically shown, and labeled at the right. Lower plot: time series of the receiving neuron.

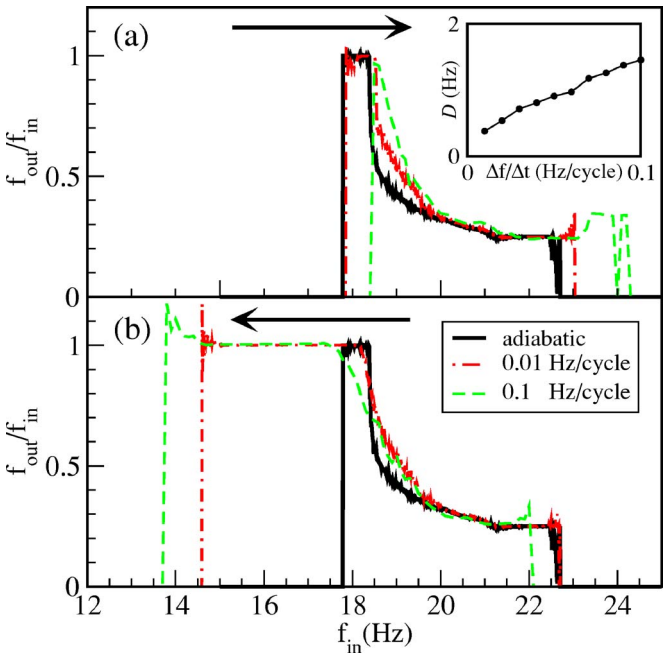

FIG. 5. (Color online) Response of a type II neuron to a controlled variation of the input frequency, for two different rates of this variation, $f'=\Delta f/\Delta t$, for g_{syn}=0.38 mS/cm^2, compared with the adiabatic response (which is a horizontal cut of the response diagram at A=0.38 mS/cm^2).

tude at zero frequency but above its minimum at resonance; this corresponds, e.g., to a horizontal line at around 0.4 mV in the right plots of Fig. 2).

Figure 4 shows what happens when the firing frequency of the input neuron first increases and then decreases in the range 13–28 Hz. The plot compares the instantaneous firing frequency of both neurons, relating them with the boundaries of the locking range of the second neuron, indicated by horizontal dashed lines; the 1:1 locking region is specifically shown. It can be seen that as the input frequency increases (first half of the plot), the receiving neuron starts spiking with approximately 1:1 frequency ratio when the input frequency falls within the corresponding locking range, the ratio decreasing when the input frequency exceeds ~20 Hz. Spiking persists while the input frequency remains in the wider (not 1:1) locking range, and is maintained even for a while after the input finally exits the locking region. A similar behavior is observed for decreasing frequencies, but the "inertia" observed at the exit of the locking region is larger than for increasing frequencies. The time series of the receiving neuron is shown in the lower plot; the episodes of synchronization with the input signal are clearly observed.

In order to understand the dynamic driving effects reported above, and particularly the locking asymmetry observed between an increase and a decrease in the input firing frequency, we now study the neuron response to a controlled variation of the frequency for different variation rates. To that end, we consider a synaptic input whose frequency is uniformly changing from one cycle to the next at a rate $f'=\Delta f/\Delta t$, and measure the response of the neuron in terms of its instantaneous output frequency f_{out}. Figure 5 shows the response diagram for a fixed synaptic strength and different frequency variation rates, for both increasing and decreasing input frequencies f_{in}. The figure shows that the slower the variation rate, the closer the response is to an adiabatic passage, as expected. Additionally, the results indicate that the persistence of the output neuron in the firing state (even when the input signal has left the locking region) is much larger when the frequency decreases than when it increases. This is consistent with the asymmetric response exhibited in Fig. 4, and can be expected to arise from the asymmetric shape of the response function f_{out}/f_{in}, which is equal to 1 for small frequencies and moderately smaller than 1 for large frequencies. Evidently the neuron prefers to respond in a 1:1 regime, which produces a larger persistence for decreasing frequencies.

To further quantify the approach to the adiabatic response in terms of the rate of change in the input frequency, we can define a distance $\mathcal{D}$ to this adiabatic response as the absolute value of the difference between the area of the neuron's response diagram at a given rate f', as plotted in Fig. 5, and the area of the adiabatic response:

$$\mathcal{D} = \int_{f_{min}}^{f_{max}} \left[\left(\frac{f_{in}}{f_{out}} \right)_{f'} - \left(\frac{f_{in}}{f_{out}} \right)_{adiab} \right] df_{in}. \qquad (14)$$

This measure is plotted in the inset of Fig. 5 as a function of the rate of change in the input frequency. The plot shows that the distance increases as the frequency changes more rapidly, as expected.

The dynamical response described in the previous paragraphs leads to episodic synchronization when the input pulse train exhibits a varying firing rate. This situation is shown in Fig. 6, in which an input pulse train whose firing rate takes the form, by way of example, of an Ornstein-Uhlenbeck noise with amplitude A_{ou}=0.1 mA and correla-

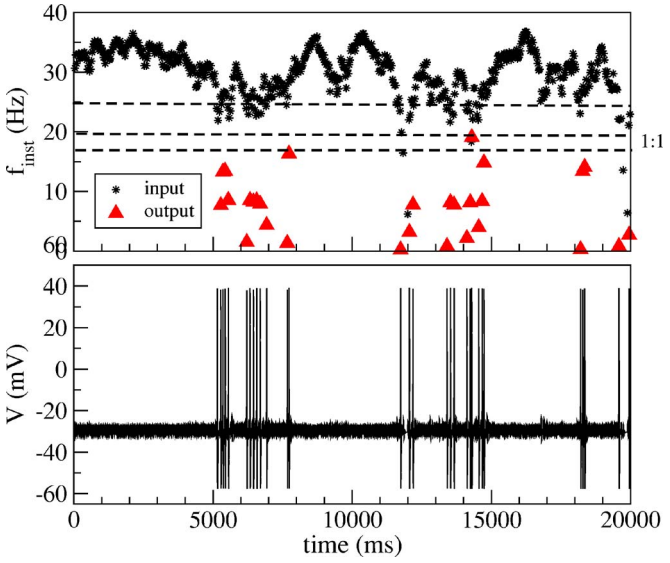

FIG. 6. (Color online) Upper panel: Instantaneous frequency of the synaptic input (black stars) and of the output neuron (triangles) as a function of time. The horizontal dashed lines delimit the region of locking according to the adiabatic calculations of Fig. 2 for the synaptic strength used (g_{syn}=0.38 mS/cm^2). Lower panel: time series of the input signal.

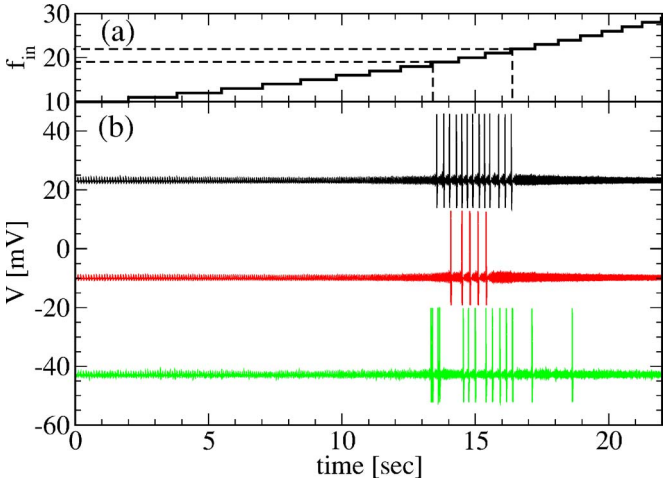

FIG. 7. (Color online) Response of a neuron to 1000 synaptic inputs with the same average frequency [increasing with time as shown in (a)]. (b) shows the response of the neuron in three cases: (top) the pulses occur synchronically, which is basically the single synapse case discussed above; (middle) the pulses are displaced in time a random amount up to $3\tau_{syn}$; (bottom) like the previous one, but with noise of intensity D=0.1 mV/ms in the applied current. In the top panel, horizontal dashed lines indicate the limits of the locking region of the neuron. In the bottom panel, the time traces are displaced vertically an arbitrary amount to ease comparison.

tion time τ_{ou}=1 s in the ~20–36 Hz range. The response of the second neuron for g_{syn}=0.38 nS is displayed in the bottom plot, and exhibits clear episodes of synchronization with the input signal, whenever the firing rate of the later falls (approximately) within the locking range of the neuron for the coupling strength chosen (represented by horizontal dashed lines in the figure). In that way the receiving neuron acts as a bandpass filter for input pulse trains.

E. Influence of multiple synaptic inputs and background noise

So far we have analyzed the rather unrealistic situation where a neuron receives a single synaptic input. But neurons are embedded in a tangled web of thousands of synaptic connections, part of which may be used by the incoming signal that the neuron is supposed to respond to, the way we have described above. The rest of synaptic connections give rise to synaptic noise. In this section, we explore the effect in the neuron's response of both multiple synaptic input trains and of background noise.

We first consider the case in which multiple information-carrying inputs act upon the neuron. Figure 7 shows the response of a neuron to 1000 trains of synaptic pulses with the same average frequency, which increases in time as shown in the top panel. The bottom panel displays the neuron's response. In the top trace, all input trains occur synchronically; this is equivalent to the single input case discussed above. When the common input frequency crosses the locking range of the neuron, indicated by dashed lines in the top panel of Fig. 7, the neuron responds. In the middle trace, the pulses are displaced randomly an amount up to $3\tau_{syn}$ and the neuron still responds in the correct frequency values, although the range is slightly smaller. Finally, in the bottom trace a Gaussian white noise of intensity D=0.1 mV/ms is added to the right-hand side of the membrane potential equation Eq. (1), representing the background activity of all other synapses that do not carry information at the selected frequency. In that case the neuron responds in a wider frequency region around the correct frequency range. This indicates that the phenomenon reported above is robust in the presence of multiple synapses.

Noise can also help the system to responsed even when the stimulus is kept below threshold. Figure 8 shows that the neuron does not fire in the absence of noise (D=0, top trace), but it does respond at a frequency around $f_{res} \simeq 21$ Hz for low noise amplitude (D=0.12 mV/ms, middle trace), and it fires at a wider range of frequencies when the noise intensity increases (D=0.18 mV/ms, bottom trace).

III. FITZHUGH-NAGUMO CIRCUIT

In order to show that the behavior reported in the previous section is generic and robust, we have reproduced the results with an electronic neuron, specifically with an electronic implementation of the FitzHugh-Nagumo (FHN) model [26]. The circuit has been previously described in [27], where synchronization between two FHN neurons was studied. A detailed description of the circuit can be found in [28]. In our particular setup, a FHN neuron is excited by a pulsed input of variable frequency.

Following the procedure of Sec. II, we first determine the response of the electronic neuron to a train of periodic pulsed inputs of fixed frequency. Specifically, we analyze the output frequency of the neuron, which is given by the inverse of the interspike interval. The input pulses have the form of square

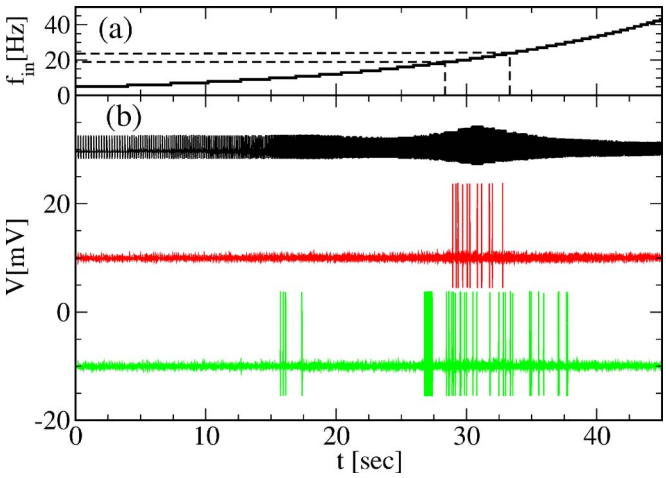

FIG. 8. (Color online) Response of the neuron in the presence of noise. (a) shows the frequency of the main synaptic input as a function of time. In (b), the upper trace shows the behavior in the absence of noise, while the middle and lower traces show the responses for Gaussian white noises of intensities $D=0.12$ mV/ms and $D=0.18$ mV/ms, respectively.

pulses of 10 ms width. Figure 9 shows the corresponding response diagram, obtained by increasing the amplitude of the input pulses until the neuron starts firing. Similar results (not shown here) are obtained with pulses of different width. At first glance, we can observe a resonance minimum around $f_{in}=15$ Hz, which confirms that the FHN neuron is of type II. Two local minima are also observed around $f_{in}=7.5$ Hz and $f_{in}=31$ Hz. It is worth noting that despite the spike threshold is low, moderately large values of the input voltage are required to induce spiking at the input frequency (see region 1:1 in Fig. 9).

We have thus a type II electronic neuron that exhibits a resonance at a frequency close to 15 Hz. Following again the approach of Sec. II, we now subject the circuit to pulse trains with time-varying frequency. Specifically, the pulse frequency is made to depend linearly with time (with both positive and negative slope). Similar results (not shown here) are obtained with sinusoidal variations. The neuron response to this dynamical input is shown in Figs. 10 and 11, where two different input voltages, corresponding to the values denoted as A and B in Fig. 9, have been applied.

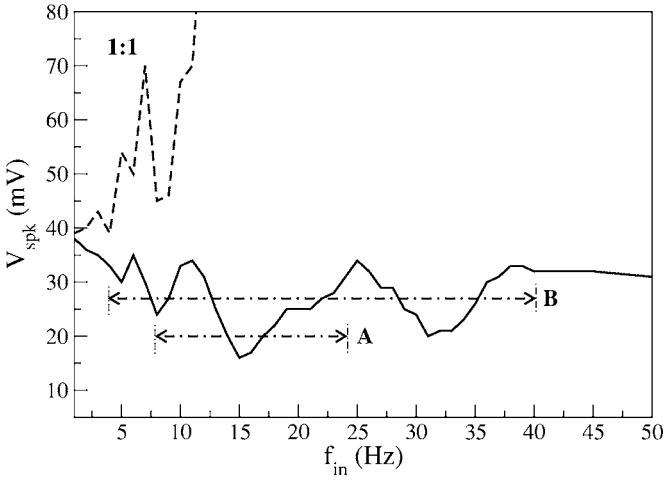

FIG. 9. Response diagram of an electronic FHN neuron for a periodic input of pulses with 10 ms width. The limit of the region of 1:1 resonance is marked with a dashed line.

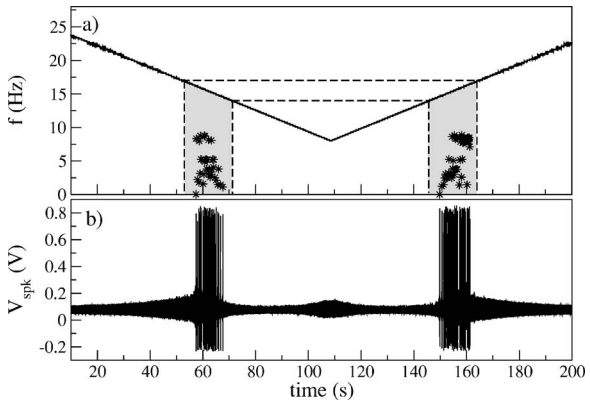

FIG. 10. Response of a FHN electronic neuron to a pulsed input of variable frequency. The input voltage corresponds to the value marked by A in Fig. 9. (a) shows the instantaneous frequency of the input pulses (solid line) and of the neuron's output (stars). The shaded region corresponds to the frequency ranges for which locking should occur. (b) displays the time evolution of the membrane voltage of the electronic neuron, which corresponds with the voltage U2 at condenser C1, in the circuit given in [28].

In the case of Fig. 10, the input signal scans the region marked with A in Fig. 9. The upper plot shows the instantaneous frequency of the input train (solid line) and of the FHN neuron (stars). Figure 10(b) plots the neuron's output. The results show that the neuron pulses when the input frequency lies within the resonance regions given in Fig. 9, and highlighted in gray in Fig. 10(a). This behavior is an agreement with the observations made in the Morris-Lecar model. The fact that no inertia effects are seen when the input frequency sweeps past the resonance region is due to the frequency variation rate being very slow with respect to the characteristic time scales of the system (adiabatic limit).

Figure 11 shows the system's behavior for a different value of the input voltage (marked as B in Fig. 9), for which

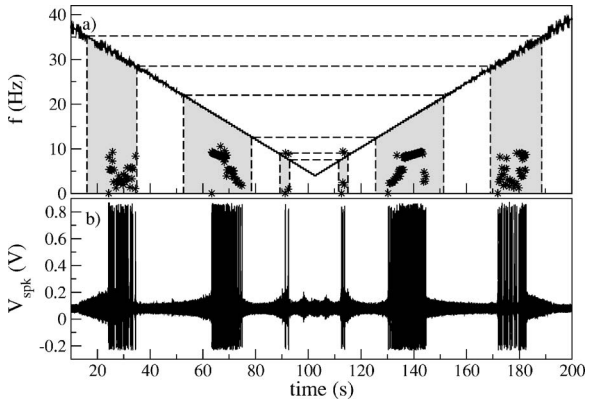

FIG. 11. Response of a FHN electronic neuron to a pulsed input of variable frequency. The input voltage corresponds to the value marked by B in Fig. 9. Figure layout is as described in the caption of Fig. 10.

the input frequency encounters three resonance regions as it varies. Accordingly, the electronic neuron fires whenever the input frequency lies inside any these regions, exhibiting clear episodes of synchronization. In other words, the neuron acts as a band-pass filter, with a frequency range that depends on the input voltage level according to its response diagram.

IV. DISCUSSION

Neurons are information-processing devices. The nature of coding in neuronal systems is still an open question. One of the important features of neuronal dynamics for information coding is the instantaneous firing rate, or time interval between spikes. Neuronal systems must therefore be able to distinguish between firing rates. We have analyzed a way to accomplish that, through the resonant behavior exhibited by type II neurons. A population of neurons with different tuning characteristics, and therefore distinct locking ranges, should be able to distinguish between different incoming pulse frequencies by activating selectively different subpopulations that respond selectively to different frequencies.

We have systematically analyzed the response of type I and II neurons to pulsed driving, compared it with the standard case of sinusoidal driving, and observed the resonant behavior of type II neurons. This phenomenology leads to episodic synchronization between the input and the output of the neuron, when the input consists of a train of pulses with dynamically varying frequency. The phenomenon has been reported both in numerical simulations of the Morris-Lecar model, and in an experimental implementation of the FitzHugh-Nagumo circuit. This behavior has been analyzed in terms of the subthreshold dynamics of the neuron, and has been seen to prevail in the presence of multiple synaptic inputs and background noise. In fact, noise helps the neuron to respond even when the stimulus is subthreshold for all frequencies.

ACKNOWLEDGMENTS

We acknowledge financial support from MCyT-FEDER (Spain, projects BFM2003-07850 and FIS2006-11452), and from the Generalitat de Catalunya. P.B. acknowledges financial support from the Fundación Antorchas (Argentina), and from a C-RED grant of the Generalitat de Catalunya. P.B. is also member of "Carrera de Conicet, Argentina."

[1] B. Lindner, J. García-Ojalvo, A. Neiman, and L. Schimansky-Geier, Phys. Rep. **392**, 321 (2004).
[2] S.-G. Lee and S. Kim, Phys. Rev. E **60**, 826 (1999).
[3] Y. Yu, F. Liu, and W. Wang, Biol. Cybern. **84**, 227 (2001).
[4] P. Parmananda, C. H. Mena, and G. Baier, Phys. Rev. E **66**, 047202 (2002).
[5] C. R. Laing and A. Longtin, Phys. Rev. E **67**, 051928 (2003).
[6] M. St-Hilaire and A. Longtin, J. Comput. Neurosci. **16**, 299 (2004).
[7] E. Puil, H. Meiri, and Y. Yarom, J. Neurophysiol. **71**, 575 (1994).
[8] B. Hutcheon and Y. Yarom, Trends Neurosci. **23**, 216 (2000).
[9] M. J. E. Richardson, N. Brunel, and V. Hakim, J. Neurophysiol. **89**, 2538 (2003).
[10] E. M. Izhikevich, Neural Networks **14**, 883 (2000).
[11] E. M. Izhikevich, BioSystems **67**, 95 (2002).
[12] E. M. Izhikevich, N. S. Desai, E. C. Walcott, and F. C. Hoppensteadt, Trends Neurosci. **26**, 161 (2003).
[13] J. M. Buldú, T. Heil, I. Fischer, M. C. Torrent, and J. Garcia-Ojalvo, Phys. Rev. Lett. **96**, 024102 (2006).
[14] C. Morris and H. Lecar, Biophys. J. **35**, 193 (1981).
[15] K. Tsumoto, H. Kitajima, T. Yoshinaga, K. Ahiara, and H. Kawakami, Neurocomputing **69**, 293 (2006).
[16] A. Destexhe, Z. F. Mainen, and T. J. Sejnowski, Neural Comput. **6**, 14 (1994).
[17] J. García-Ojalvo and J. M. Sancho, *Noise in Spatially Extended Systems* (Springer, New York, 1999).
[18] J. Xie, J.-X. Xu, Y.-M. Kang, S.-J. Hu, and Y.-B. Duan, Chin. Phys. **13**, 1396 (2004).
[19] In top left panel of Fig. 2, the spiking region stretches down below $A=0.3$ nS, a lower value than expected. This happens because the amplitude of the synaptic pulses is larger than A, due to modulation by the term $(V-E_s)$ shown in Eq. (7).
[20] E. Puil, B. Gimbarzevsky, and R. M. Miura, J. Neurophysiol. **55**, 995 (1986).
[21] Y. Gutfreund, Y. Yarom, and I. Segev, J. Physiol. (London) **483**, 621 (1995).
[22] B. Hutcheon, R. M. Miura, and E. Puil, J. Neurophysiol. **76**, 683 (1996); **76**, 698 (1996).
[23] L. S. Leung and H. W. Yu, J. Neurophysiol. **79**, 1592 (1998).
[24] F. G. Pike, R. S. Goddard, J. M. Suckling, P. Ganter, N. Kasthuri, and O. Paulsen, J. Physiol. (London) **529**, 205 (2000).
[25] We have considered, in the subthreshold analysis presented here, that the pulsed input current is not modulated by the postsynaptic membrane potential, as it should be in the case of a synaptic input [see Eq. (7)]. This approximation considers that the pulsed input is an electrically applied current, analogous to the harmonic current analyzed earlier.
[26] J. Nagumo, S. Arimoto, and S. Yoshizawa, Proc. IRE **50**, 2061 (1962).
[27] R. Toral, C. Masoller, C. R. Mirasso, M. Ciszak, and O. Calvo, Physica A **325**, 192 (2003).
[28] http://www.fen.upc.edu/donll/info/FHNcircuit.pdf.